Supplementary Information

Directed nucleation and growth by balancing local supersaturation and substrate/nucleus lattice mismatch

L. Li,[1,2,3] A. J. Fijneman,[1,4] J. A. Kaandorp,[5] J. Aizenberg,[1,2,6,7] W. L. Noorduin,[1,8]

[1]John A. Paulson School of Engineering and Applied Sciences, Harvard University, Cambridge, MA 02138, USA
[2]Wyss Institute for Biologically Inspired Engineering, Harvard University, Boston, MA 02115, USA
[3]Department of Mechanical Engineering, Virginia Polytechnic Institute and State University, Blacksburg, VA 24060, USA
[4]Department of Chemical Engineering and Chemistry, Eindhoven University of Technology, 5612 AZ Eindhoven, The Netherlands
[5]Computational Science Lab, Faculty of Science, University of Amsterdam, 1098 XH Amsterdam, The Netherlands
[6]Kavli Institute for Bionano Science and Technology, Harvard University, Cambridge, MA 02138, USA
[7]Department of Chemistry and Chemical Biology, Harvard University, Cambridge, MA 02138, USA
[8]AMOLF, 1098 XG Amsterdam, The Netherlands.

Content

1. Simultaneous crystallization of calcite, aragonite, and vaterite
2. Overgrowth of a $CaCO_3$ polymorph mixture with $BaCO_3$
3. Overgrowth of a $CaCO_3$ polymorph mixture with $SrCO_3$
4. Overgrowth of a $CaCO_3$ polymorph mixture with $BaCO_3/SiO_2$ microstructures
5. Overgrowth of a $CaCO_3$ polymorph mixture with $CaCO_3$/PAA microstructures
6. FIB/TEM procedure
7. Crystal structure analysis
8. Calculations of lattice mismatch
9. Derivation of equation 2

1. Simultaneous crystallization of calcite, aragonite, and vaterite

For the crystallization of mixed polymorphs of $CaCO_3$, 0.032 g of $CaCl_2$ was dissolved in 15 mL water in a 50 or 100 mL beaker. An aluminum slide (ca. 15x15x1 mm), or aluminum-coated microscope glass slide, was vertically positioned in the solution and the beaker was placed in a closed desiccator with freshly ground $(NH_4)_2CO_3$ following the method developed by Addadi *et al.* (*1*). After ca. 30-45 min, the slide was removed from the solution, washed twice with water and then washed with acetone and dried on the air. Optical microscopy, scanning electron microscopy (SEM) and Raman microscopy revealed that the slide contained a mixture of calcite (79±8%), aragonite (14±5%) and vaterite (7±3%) (Fig. SI 1).

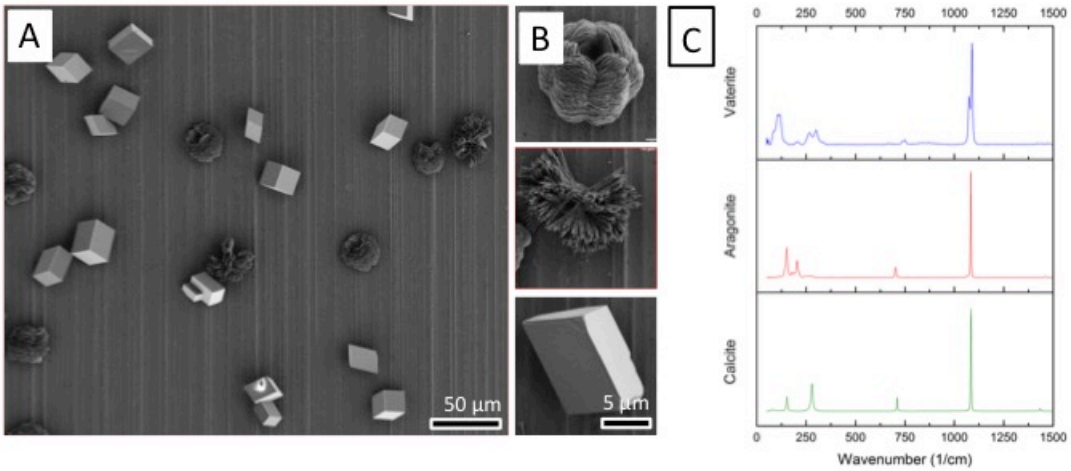

Figure SI 1. Crystallization of calcite, aragonite and vaterite. (A) SEM image of a typical sample area containing a mixture of vaterite, aragonite and calcite. (B) Close up SEM images of vaterite, aragonite and calcite (top to bottom). (C) Raman spectra absorption spectra of vaterite, aragonite and calcite crystals excited at 514 nm.

2. Overgrowth of a $CaCO_3$ polymorph mixture with $BaCO_3$

In a 50 or 100 mL beaker, we dissolved 0.074 g $BaCl_2$ in 15 mL water and adjusted the pH to 11.9 using NaOH. A previously prepared slide with a mixture of calcite, aragonite and vaterite (see above) was positioned at a 90º angle in the solution such that a half of the previously overgrown area (shown schematically as a green line in Fig. SI2A, left) was submerged. A petri dish was loosely placed on the beaker allowing for the CO_2 from the air to enter the beaker. After ca. 30-45 min, the slide was removed from the solution, washed twice with water and then washed with acetone and subsequently dried. Optical microscopy and SEM were used to analyze the slide and quantify the crystallization of the $BaCO_3$ on the $CaCO_3$ mixture (shown schematically as a red line in Fig. SI 2A, left). To quantify the polymorphic overgrowth, we manually counted each polymorph as a function of the depth. Subsequently we plotted the cumulative distribution function. Alternatively, we define the polymorph overgrowth ratio $R_{Ba,x}$ for a specific $CaCO_3$ polymorph x as $R_{Ba,x} = (n_{Ba,x}/n_x)/\Sigma_{x'}(n_{Ba,x'}/n_{x'})$, with n_x denoting the total number of $CaCO_3$ crystals of the polymorph, $n_{Ba,x}$ the number of $CaCO_3$ crystals of this polymorph that have been overgrown with $BaCO_3$, and the sum in the nominator running over all possible polymorphs.

The CDF is computed by manually counting the overgrown $CaCO_3$ crystals per polymorph as a function of the depth as a fraction of the total number of overgrown $CaCO_3$ crystals. Note that the CDF does not include the data of the $CaCO_3$ crystals that are not overgrown.

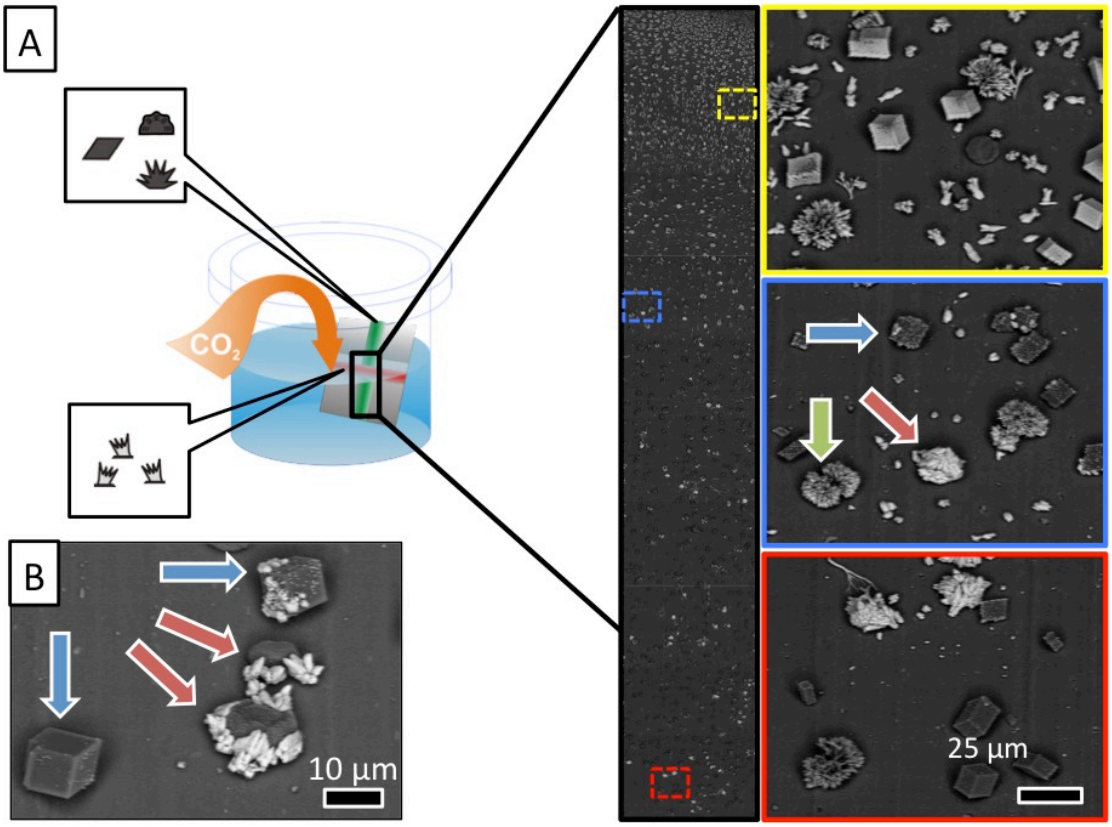

Figure SI 2. Analysis of overgrowth of a $CaCO_3$ polymorph mixture with $BaCO_3$. (A) Left: Schematic drawing showing the positioning of the substrate containing the mixture of $CaCO_3$ polymorphs (green line and the inset on the top) that becomes overgrown with $BaCO_3$ (red line and the lower inset). Right: Backscatter SEM images, in which $BaCO_3$ appears light and $CaCO_3$ appears dark, qualitatively show that at the top (yellow box) calcite and aragonite are overgrown, deeper in the solution (blue box) all three polymorphs are overgrown and at the deepest part (red box) mainly vaterite crystals are overgrown. (B) Backscatter SEM image taken at the deepest part in the solution (2.5-3.0mm) showing two overgrown vaterite crystals (red arrow). The local increase in the $[CO_3^{2-}]$ from the dissolving vaterite crystals also caused crystallization on a calcite crystal that grew in the immediate vicinity of vaterite; note that the overgrowth of $BaCO_3$ on this crystal takes place on the surface facing the nearby vaterite (top blue arrow), whereas a calcite crystal further away from the vaterite crystals remains empty (bottom blue arrow).

3. Overgrowth of a $CaCO_3$ polymorph mixture with $SrCO_3$

In a 50 or 100 mL beaker we dissolved 0.084 g of $SrCl_2$ in 15 mL water and adjusted the pH to 11.9 using NaOH. A similar procedure was followed as for $BaCO_3$ as described above. Optical microscopy and SEM were used to analyze the results and quantify the crystallization of the $SrCO_3$ on the $CaCO_3$ mixture (Fig. SI 3).

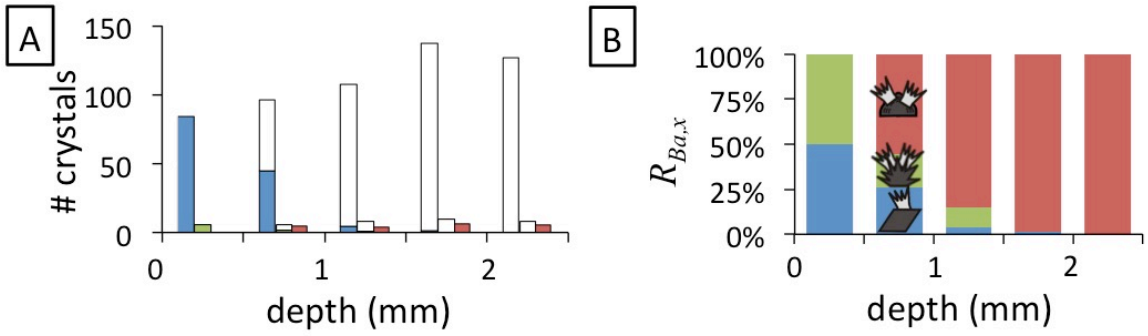

Figure SI 3. Analysis of overgrowth of a $CaCO_3$ polymorph mixture with $SrCO_3$. (A) Number of $CaCO_3$ crystals as a function of the depth: calcite (left clear bar), aragonite (middle clear bar) and vaterite (right clear bar), and number of overgrown $CaCO_3$ crystals: calcite-$SrCO_3$ (left blue bar), aragonite-$SrCO_3$ (middle green bar) and vaterite-$SrCO_3$ (right red bar). (B) Polymorph overgrowth ratio $R_{Ba,x}$ based on data in Fig. SI 3A.

4. Overgrowth of a $CaCO_3$ polymorph mixture with $BaCO_3/SiO_2$ microstructures

In a 50 or 100 mL beaker, we dissolved 0.074 g of $BaCl_2$ and 0.016 g of Na_2SiO_3 in 15 mL water. To grow structures in the blossoming regime, the pH was adjusted to pH 11.9 whereas for growth in the curling regime the pH was adjusted to 11.1 (*2*). A previously prepared slide with a mixture of calcite, aragonite and vaterite (see above) was positioned at 90º in the solution such that half of the previously overgrown area was submerged in the solution. A petri dish was loosely placed on the beaker such that CO_2 from the air could enter the beaker. After ca. 45 – 120 min, the slide was removed from the solution, washed twice with water and then washed with acetone and dried in the air. Optical microscopy and SEM were used to analyze the results.

5. Overgrowth of a $CaCO_3$ polymorph mixture with $CaCO_3$/PAA microstructures

In a 50 or 100 mL beaker, we dissolved 0.032 g of $CaCl_2$ and between 60 and 120 μg/mL poly (α,L-aspartate) (Sigma Aldrich) in 15 mL water. A previously prepared slide with a mixture of calcite, aragonite and vaterite (see above) was position under positioned at 90º in the solution such that half of the previously overgrown area was submerged. The beaker was placed in a closed desiccator with freshly ground $(NH_4)_2CO_3$ and placed in an oven at 45 °C. After ca. 45 – 120 min, the slide was removed from the solution, washed twice with water and then washed with acetone and dried in the air. Optical microscopy, Raman microscopy and SEM were used to analyze the slide.

6. FIB/TEM procedure

Samples were coated with Au (~5 nm) to reduce charging effects prior to focused ion beam (FIB) milling with a Helios Nanolab 660 Dual Beam electron microscope (FEI, OR). Typical TEM sample preparation procedure was as follows: 1) a platinum protective layer (~0.5 μm) was first laid down on top of the desired structure; 2) another platinum protective layer (~1.5 μm) was further deposited on top of the rectangular region where the TEM slab was to be milled out; 3) two sides of the coated structure, were milled away by FIB, leaving the slab of specimen (thickness: ~1.5 μm); 4) the slab was then cut through by FIB and transferred to a copper TEM grid by an Omniprobe and welded securely with platinum deposition; 5) the lift-out lamellar of specimen was

sequentially thinned by FIB at 30, 16, 5, and 2 kV ion beam voltages. Final cleaning at 2 kV and 28 pA is important to obtain a clean surface and minimize damage. TEM imaging was carried out using a JEOL 2011 operated at 120 kV.

7. Crystal structure Analysis

Table SI 1: Crystallographic information for various $CaCO_3$ polymorphs, $BaCO_3$ and $SrCO_3$.

Substance	Polymorph (Common name)	Crystal system	Space group	a/Å	b/Å	c/Å	α/(°)	β/(°)	γ/(°)
$CaCO_3$	Calcite	Trigonal	$R\bar{3}c$	4.988	4.988	17.061	90	90	120
	Aragonite	Orthorhombic	Pmcn	4.961	7.967	5.741	90	90	90
	Vaterite	Hexagonal	P63/mmc	7.290	7.290	25.302	90	90	120
$BaCO_3$	Witherite	Orthorhombic	Pmcn	5.313	8.896	6.428	90	90	90
$SrCO_3$	Strontianite	Orthorhombic	Pmcn	5.090	8.358	5.997	90	90	90

Calcite/$BaCO_3$

Based on TEM/diffraction studies (Fig. 2 and Fig. SI 4), the *c*-axes of the two types of crystals are aligned. Diffraction results also suggest that the $(10\bar{1}0)$ planes of calcite are aligned with (010) planes of $BaCO_3$. Although it was not explicitly stated, similar diffraction results were obtained by Wu *et al.* (*3, 4*) for the cases of Ca-doped $SrCO_3$ and $BaCO_3$ on the substrate of calcite, respectively.

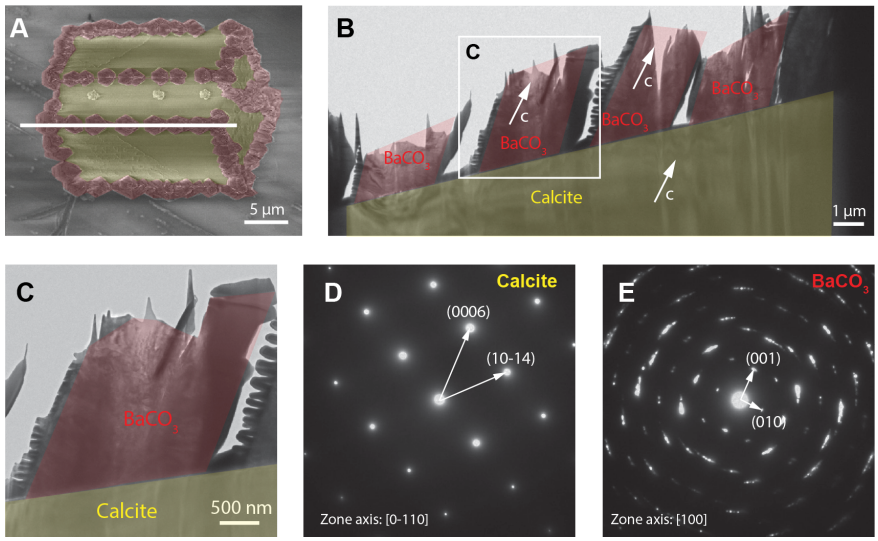

Fig. SI 4. Structural analysis of calcite/$BaCO_3$ interface. (A) Top-view SEM image of the original calcite crystal overgrown with $BaCO_3$ crystals. The white line indicates the location and orientation of the TEM sample prepared via FIB milling. (B) Overview TEM image of the overgrowth of multiple $BaCO_3$ crystals (red regions) on calcite (yellow region). The top portions of $BaCO_3$ crystals were milled away during FIB polishing. (C) A representative TEM image of $BaCO_3$/calcite interface. Selected area electron diffraction patterns of underlying calcite substrate and overgrown $BaCO_3$ crystal acquired from regions in (C).

Aragonite/$BaCO_3$

TEM analysis showed that the crystallographic axes of $BaCO_3$ and aragonite are aligned (Fig. 2 and Fig. SI 5).

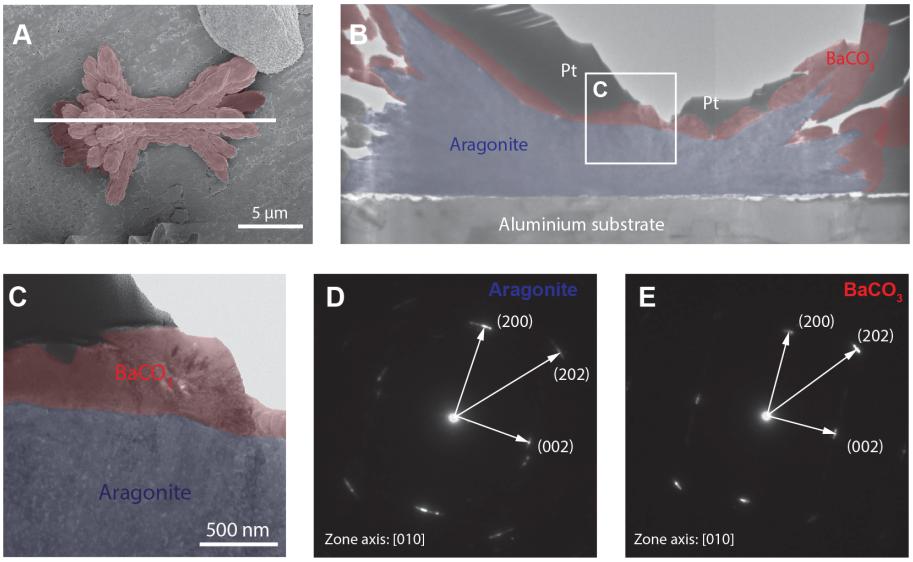

Fig. SI 5. Structural analysis of aragonite/$BaCO_3$ interface. (A) Top-view SEM image of the original aragonite crystal overgrown with $BaCO_3$ crystals. The white line indicates the location and orientation of the TEM sample prepared via FIB milling. (B) Overview TEM image of the overgrowth of $BaCO_3$ crystals (red regions) on aragonite (blue region). (C) A representative TEM image of $BaCO_3$/aragonite interface. Selected area electron diffraction patterns of underlying aragonite substrate and overgrown $BaCO_3$ crystal acquired from regions in (C).

Vaterite/$BaCO_3$

The vaterite crystals have their *c*-axis perpendicular to the microplates and the *a*-axis is parallel to the growth direction as shown in the hexagonal-shaped crystal used for TEM imaging shown in Fig. 2A, column iv and Fig. SI 6. This has been observed in a previous report (*5*). Electron diffraction studies in multiple locations at the vaterite/$BaCO_3$ interface do not show a consistent correlation for the crystal orientations in vaterite and $BaCO_3$.

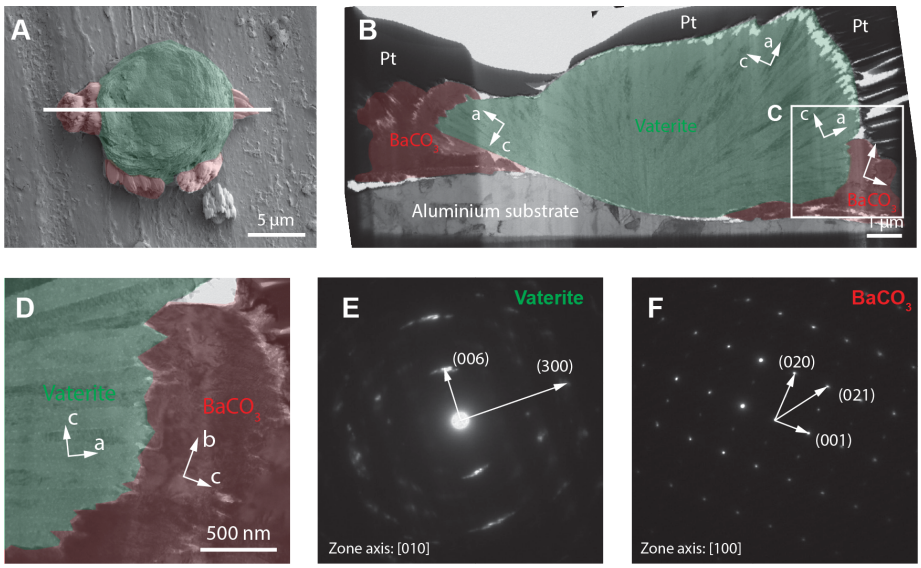

Fig. SI 6. Structural analysis of vaterite/$BaCO_3$ interface. (A) Top-view SEM image of the original vaterite crystal overgrown with $BaCO_3$ crystals. The white line indicates the location and orientation of the TEM sample prepared via FIB milling. (B) Overview TEM image of the

overgrowth of $BaCO_3$ crystals (red regions) on vaterite (blue region). (C) A representative TEM image of $BaCO_3$/vaterite interface. Selected area electron diffraction patterns of vaterite and overgrown $BaCO_3$ crystals acquired from regions in (C).

8. Calculations of crystal lattice mismatch

Based on the structural analysis in the previous session, we are able to determine the lattice mismatch between overgrowth crystals ($BaCO_3$ and $SrCO_3$) and different $CaCO_3$ polymorph crystals (calcite and aragonite) as substrates (**Fig. SI 7**). Here we adopt a similar approach reported by Pokroy and Zolotoyabko (*6*) in estimating lattice mismatches in both ***a*** and ***b*** directions. For the case of aragonite as a substrate, the mismatch M^a and M^b can be calculated according to the equations below

$$M^a = \frac{a_{overgrowth} - a_{substrate}}{a_{substrate}}$$

and

$$M^b = \frac{b_{overgrowth} - b_{substrate}}{b_{substrate}}$$

The average lattice mismatch is defined as

$$|\bar{M}| = (|M^a| + |M^b|)/2$$

For the case of calcite as a substrate, which is a rhombohedral crystal, the equivalent ***b**** of the orthorhombic unit cell (**Fig. SI 5**) is

$$b^* = \sqrt{3}a$$

Then the lattice mismatch can be calculated by using the same relationships above by replacing ***b*** with ***b****.

The calculated mismatch values are tabulated in **Table SI 2**. It is noted that for both overgrowth of $BaCO_3$ and $SrCO_3$, the lattice mismatch in both ***a*** and ***b*** directions is slightly smaller for the case of calcite as the substrate in comparison to the case of aragonite as the substrate.

Table SI 2: Crystal lattice mismatch between substrate (calcite and aragonite) and overgrowth ($BaCO_3$ and $SrCO_3$) crystals. The relevant parameters are defined in the text.

Type	Substance	Crystal system	a/Å	b/Å	b*/Å	Calcite as substrate			Aragonite as substrate		
Substrate	Calcite	Trigonal	4.988	4.988	8.6395	M^a	M^b	$\|\bar{M}\|$	M^a	M^b	$\|\bar{M}\|$
	Aragonite	Orthorhombic	4.961	7.967	7.967						
Overgrowth	$BaCO_3$	Orthorhombic	5.313	8.896	8.896	0.0652	0.0297	**0.0474**	0.0710	0.1166	**0.0938**
	$SrCO_3$	Orthorhombic	5.090	8.358	8.358	0.0204	0.0326	**0.0265**	0.0260	0.0491	**0.0375**

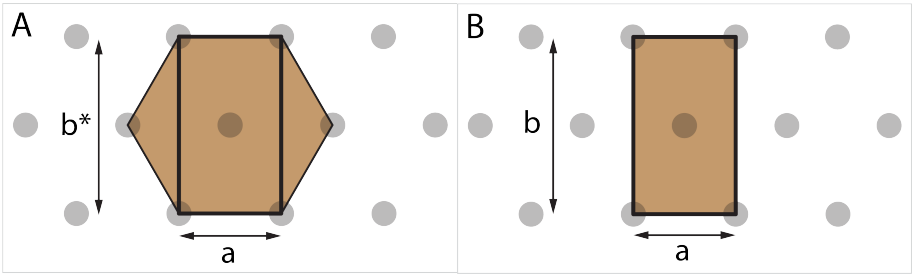

Fig. SI 7. Schematic diagram of cation (indicated by the gray dots) arrangement in the (001) plane of rhombohedral (calcite) and orthorhombic (aragonite, $BaCO_3$ and $SrCO_3$) crystals. Note for the case calcite as substrate, the $(10\bar{1}0)$ planes of calcite are aligned with (010) planes of $BaCO_3$, as observed from the TEM and electron diffractions.

9. Derivation of equation 2

For the derivation of equation 2, we start by defining a rate equation for the local carbonate concentration $[CO_3^{2-}]_{local}$ from the dissolution of the different calcium carbonate polymorphs $CaCO_{3x}$. According to Plummer *et al.* (*7,8*) the dissolution rate v_{net} of $CaCO_3$ can be described as:

$$v_{net} = k_1 a_{H^+} + k_1 a_{HCO_3^-} + k_3 a_{H_2O} - k_4 a_{Ca^{2+}} a_{HCO_3^-} \quad (1)$$

where a_x denotes the bulk solution activity of species x and k_1, k_2, k_3, and k_4 are rate constants. A modified version of the Plummer *et al.* model also contains the dissolution/precipitation of calcite and aragonite (*9,10*). According to this modified model the dissolution of calcite in three regions of pH is controlled by the following reactions:

$$\begin{aligned} &CaCO_3 + H^+ \rightleftarrows HCO_3^- \\ &CaCO_3 + H_2CO_3 \rightleftarrows Ca^{2+} + 2HCO_3^- \\ &CaCO_3 \rightleftarrows Ca^{2+} + CO_3^{2-} \end{aligned} \quad (2)$$

For pH > 7 a rate reaction equation was derived from the Plummer model describing the dissolution rate (*10-12*):

$$v_{net} = k_x - k_x'[Ca^{2+}]_s[CO_3^{2-}]_s \quad (3)$$

where $k_x' = k_x/K_{sp\text{-}CaCO3x}$ with the solubility product $K_{sp\text{-}CaCO3x}$, and k_x is the dissolution rate constant of $CaCO_3$ which depends on the surface morphology of the dissolving crystal and on the specific polymorph x. The subscript s denotes the concentrations in the surface layers near the dissolving calcium carbonate crystal. The values for k_x' and k_x correspond to the values of k_3 and k_4 in the Plummer model. When we use k_x in equation 3 for the specific polymorphs of calcium carbonate, then we can assume $k_{vaterite} > k_{aragonite} > k_{calcite}$ and $K_{sp,vaterite} > K_{sp,aragonite} > K_{sp,calcite}$. Please note that for the regime we consider the dissolution rate is positive, i.e. $k_x > k_x/K_{sp\text{-}CaCO3x}[Ca^{2+}][CO_3^{2-}]$.

Using this expression for the dissolution rate of calcium carbonate, we can now formulated the local concentration of CO_3^{2-} in time during the nucleation of $BaCO_3$, while the underlying $CaCO_3$ crystal is dissolving and additional influx of CO_3^{2-} occurs from the bulk solution. When we assume that the contribution of reverse reactions is very

small and we do not consider diffusion, the rate equation for the carbonate concentration around the nucleating $BaCO_3$ crystal $[CO_3^{2-}]_{local}$ can be expressed as:

$$\frac{d[CO_3^{2-}]_{local}}{dt} = k_{influx}[CO_3^{2-}]_{bulk} + k_x - k_x'[Ca^{2+}]_s[CO_3^{2-}]_s - k_{BaCO_3}[Ba^{2+}][CO_3^{2-}]_{local} \quad (4)$$

where k_{influx} is a rate constant describing the influx of CO_3^{2-} from the bulk solution towards the nucleating $BaCO_3$ crystal, and k_{BaCO3} the crystallization rate constant.
The dissolution term for $CaCO_{3,x}$ is described by equation (3). Since the growth of the crystal is relatively slow compared to the diffusion of $[CO_3^{2-}]_{local}$, we can assume a steady state in $[CO_3^{2-}]_{local}$:

$$\frac{d[CO_3^{2-}]_{local}}{dt} = 0 \quad (5)$$

Furthermore, we can assume $[CO_3^{2-}]_{local} = [CO_3^{2-}]_s$ since nucleation of $BaCO_3$ occurs on the surface of the $CaCO_3$, such that equation (4) changes into:

$$k_{influx}[CO_3^{2-}]_{bulk} = -k_x + k_x'[Ca^{2+}]_s[CO_3^{2-}]_{local} + k_{BaCO_3}[Ba^{2+}][CO_3^{2-}]_{local} \quad (6)$$

$$\frac{k_{influx}[CO_3^{2-}]_{bulk}}{[CO_3^{2-}]_{local}} = k_{BaCO_3}[Ba^{2+}] - k_x + k_x'[Ca^{2+}]_s \quad (7)$$

$$[CO_3^{2-}]_{local} = \frac{k_{influx}[CO_3^{2-}]_{bulk}}{k_{BaCO_3}[Ba^{2+}] - k_x + k_x'[Ca^{2+}]_s} \quad (8)$$

with k_{BaCO3} the crystallization rate constant of $BaCO_3$. The formation of $BaCO_3$ under supersaturated conditions is described by:

$$\frac{d[BaCO_3]}{dt} = k_{BaCO_3}[Ba^{2+}][CO_3^{2-}]_{local} \quad (9)$$

Substitution of (8) into (9) gives:

$$\frac{d[BaCO_3]}{dt} = \frac{k_{BaCO_3}[Ba^{2+}]k_{influx}[CO_3^{2-}]_{bulk}}{k_{BaCO_3}[Ba^{2+}] - k_x + k_x'[Ca^{2+}]_s} \quad (10)$$

The free energy of the solution per molecule is (*13,14*):

$$\Delta g_{sol} = -k_B T \ln K_{sp-BaCO_3} \quad (11)$$

The change in chemical potential is given by (*13,14*):

$$\Delta\mu = k_B T \ln\left(\frac{[Ba^{2+}][CO_3^{2-}]_{local}}{K_{sp-BaCO_3}}\right) \quad (12)$$

and the supersaturation σ can be written as:

$$\sigma = \ln(\frac{[Ba^{2+}][CO_3^{2-}]_{local}}{K_{sp-BaCO_3}}) \quad (13)$$

where k_B is the Boltzmann constant, K_{sp_BaCO3} is the solubility product of $BaCO_3$ and T is the absolute temperature.

Since $[CO_3^{2-}]_{local}$ depends on $[CO_3^{2-}]_{bulk}$, $[Ba^{2+}]$, and $[Ca^{2+}]$s (see Eq. 8), it is useful to substitute Eq. 8 into Eq. 13 and set k_{influx} to unity. Furthermore, we use the relation for the equilibrium constant K_c,:

$K_c = \frac{k_{BaCO_3}}{k_-} = \frac{[BaCO_3]_{eq}}{[Ba^{2+}]_{eq}[CO_3^{2-}]_{eq}}$, with k_- the dissolution rate constant of $BaCO_3$. By substituting $K_{sp\_BaCO_3} = [Ba^{2+}]_{eq}[CO_3^{2-}]_{eq}$ and setting the activity of the solid $[BaCO_3]_{eq}$ and k_- to unity leads to: $K_{sp-BaCO_3} \approx \frac{1}{k_{BaCO_3}}$, such that the supersaturation can be written as:

$$\sigma = \ln\left(\frac{k_{BaCO_3}[Ba^{2+}][CO_3^{2-}]_{bulk}}{k_{BaCO_3}[Ba^{2+}] - k_x + k_x'[Ca^{2+}]_s} \right) . \quad (14)$$

References

1. L. Addadi, J. Moradian, E. Shay, N. G. Maroudas, S. Weiner, *Proc. Natl. Acad. Sci.* ***84,*** 2732-2736 (1987).
2. W.L. Noorduin, A. Grinthal, L. Mahadevan, J. Aizenberg, *Science* ***340,*** 832-837 (2013).
3. W. Wu, Y. Ma, Y. Xing, Y. Zhang, H. Yang, Q. Luo, J. Wang, B. Li, L. Qi, *Cryst. Growth Des.* ***15,*** 2156-2164 (2015).
4. W. Wu, Y. Zhang, B. Li, Y. Ma, *Acta Phys. –Chim. Sin.* ***31***, 189-198 (2015).
5. Q. Hu, J. Zhang, H. Teng, U. Becker, *Amer. Miner.* ***97,*** 1437–1445 (2012).
6. B. Pokroy and E. Zolotoyabko, *Chem. Comm.* 2140-2142 (2005).
7. L.N. Plummer, D.L. Parkhurst, T.M.L. Wigley, *ACS Symposium Series****, 93,*** 537-573 (1979).
8. L.N. Plummer, T.M.L. Wigley, D.L. Parkhurst, *Amer. J. Sci.* ***278,*** 179-216 (1978).
9. L. Chou, R.M. Garrels, R. Wollast, *Chem. Geol.* ***78,*** 269-282 (1989).
10. R.G. Compton, K.L. Pritchard, *Phil. Trans. Roy. Soc. London,* ***A330,*** 47-70 (1990).
11. W.P. Inskeep and P.R. Bloom, *Geochimica et Cosmochimica,* ***49,*** 2165-2180, (1985).
12. B. Sanjuan, J.P. Girard, *Review of kinetic data on carbonate mineral precipitation*, *BRGM Report R39062*, 1-91 (1996).
13. A.A. Chernov, (1984). Modern Crystallography III: Crystal Growth. *Springer, Berlin* 978-3-642-81835-6.
14. J.J. De Yoreo, P.G Vekilov, P. M. Dove, Weiner Eds, S. (2003) Principles of crystal nucleation and growth. In Biomineralization 57-93. *Mineral Soc. Am., Washington, DC* 10.2113/054005.